



Should Gold Marker or TEM-ASTAR Characterization Be Used to Determine Oxide Growth Direction?

L. Latu-Romain^{1,2} · T. Roy¹ · T. Perez³ · Y. Parsa¹ · L. Aranda³ · R. Podor⁴ · S. Mathieu³ · M. Vilasi³ · Y. Wouters¹

Received: 25 May 2021 / Revised: 25 May 2021 / Accepted: 29 May 2021 /
Published online: 21 July 2021

© The Author(s), under exclusive licence to Springer Science+Business Media, LLC, part of Springer Nature 2021

Abstract

Oxidation of chromia-forming alloys (pure chromium, nickel–chromium alloy and ferritic stainless steel alloy) at temperature ranging from 800 to 1050 °C was conducted on samples with or without gold markers applied prior to testing. Gold is often used as a marker in order to identify oxide growth direction. Its localization inside the oxide scale can demonstrate an inward or an outward growth. It is found that gold particles can be found either at the internal metal/oxide interface or inside the scale or again at the external oxide/gas interface on the same sample (on NiCr and stainless steel alloys). For pure chromium oxidation, gold is found inside the chromia scale, at the equiaxed-columnar interface, as expected from ASTAR-TEM characterization. However, photoelectrochemical characterization has shown that gold can modify the semiconducting chromia properties. Finally, gold is not inert in these several conditions and should not be considered in these present cases, but also more generally in most cases, as an appropriate marker. On the contrary, ASTAR maps may permit to access the oxide growth direction without interfering the studied system.

Keywords Marker · Photoelectrochemistry · TEM-ASTAR · Chromia-former alloys · High-temperature oxidation

✉ L. Latu-Romain
laurence.latu-romain@univ-grenoble-alpes.fr

¹ CNRS, Grenoble INP, SIMaP, Univ. Grenoble Alpes, 38000 Grenoble, France

² UGITECH, Avenue Paul Girod, 73400 Ugine, France

³ IJL, University of Lorraine, Nancy, France

⁴ ICSM, CEA, CNRS, ENSCM, Univ Montpellier, Bagnols sur Cèze, France

Introduction

This paper is focused on the use of gold as markers to assess the oxide growth direction on chromia-former alloys. Indeed, in the high-temperature oxidation research field, knowing the oxide growth direction is one of the key points for the oxide edification understanding. An inward growth is governed by anionic point defects diffusion (as oxygen vacancies or interstitials), whereas an outward growth is governed by cationic point defects (as metallic vacancies or interstitials). The major point defect nature can finally be given only if the type of conduction is additionally characterized. The latter can be determined by electrochemical characterization techniques as Mott–Schottky or photoelectrochemistry. The oxide growth direction can be determined by alternative $^{16}\text{O}_2/^{18}\text{O}_2$ oxidation experiments or, in a simple manner, by the use of marker priory deposited on the metallic surface. Two-stage oxidation experiments under successive exposures in $^{16}\text{O}_2$, and then $^{18}\text{O}_2$, followed by secondary ion mass spectrometry (SIMS) and sputtered neutral mass spectrometry (SNMS) permit to sign the oxide growth direction as a function of ^{18}O profile [1, 2]. Described in the thirties by Pfeil [3], the experiment with markers is based on the observation after oxidation of the position of inert markers (small particles of Pt, Au, SiO_2 and Al_2O_3) deposited on the surface before oxidation [4]. Gold or platinum is often chosen because it is claimed to be inert [5–7]. The former is generally preferred since platinum exhibits catalytic activity for many chemical reactions [8]. When dense oxide scales are formed, the position of the marker is indicative of the diffusion process. A transversal cross section inside the oxide scale permits to localize the marker which should indicate the position of the initial metal-atmosphere interface. If markers are localized at the internal metal/oxide interface (resp. external oxide/gas interface), it means that the oxide growth direction is external (resp. internal).

In this study a careful look of the incidence of the use of gold markers for oxide growth direction determination will be shown with the example of several chromia-former materials: from pure chromium until AISI 441 stainless steel passing by NiCrMn model alloys.

Experimental Procedures

Pure chromium (99.99% purity, from Goodfellow SARL, France) had been oxidized in a low oxygen partial pressure of 10^{-14} atm. at 800 °C during 1 h. Before oxidation experiments, Cr samples were cut to the dimension $10 \times 10 \times 1$ mm³ and were SiC-ground up to the grade 320. Rhines pack procedure had been further employed in order to fix the oxygen partial pressure. This technique has been largely described elsewhere [9, 10]. In this example, Ni/NiO powders had been chosen and fixed a $p(\text{O}_2)$ of 10^{-14} atm. at 800 °C. In these conditions, oxide scale thickness was estimated inferior to one micrometer, the suited range to perform ex situ photoelectrochemical experiments. It should be noted that this experiment

had been carried out in order to determine semiconducting chromia properties as a function of oxygen activity.

$\text{Ni}_{74.5}\text{Cr}_{25}\text{Mn}_{0.5}$ and $\text{Ni}_{74}\text{Cr}_{25}\text{Mn}_1$ (in wt%) model alloy was prepared by high-frequency melted under argon gas and then heat-treated for 12 h at 1000 °C under argon for homogenization and to avoid segregation. $\text{Ni}_{74.5}\text{Cr}_{25}\text{Mn}_{0.5}$ alloy was oxidized in an environmental scanning electron microscope (FEI Quanta 200 FEG ESEM) equipped with a hot stage under an atmosphere of pure O_2 . The hot stage was heated to the experimental temperature of 1050 °C under 1.97×10^{-3} atm. during 1 h. (Experimental details can be found elsewhere [11].) $\text{NiCr}_{25}\text{Mn}_1$ was also oxidized at 1050 °C during 100 h at atmospheric pressure.

The ferritic stainless steel (441, with composition indicated in Table 1) had been oxidized at 900 °C during 10 h and 100 h at atmospheric pressure in a tubular furnace under synthetic air followed by an air quench.

Concerning these experiments, it should be underlined that the effect of Mn on NiCr model alloy or on ferritic stainless steel oxidation was also carefully studied but does not concern the purpose of the present paper.

Thin gold films with a thickness of 1–3 nm had been deposited on some Cr, NiCrMn and 441 samples by physical vapor deposition. It should be additionally noted that dewetting of the gold film was performed during the heating of the samples during oxidation and led to gold solid droplets of about 200 nm in diameter distributed on the surface.

The photoelectrochemical characterization technique has been intensively described and recently discussed [12, 13]. In a few words, this method consists of the electron–hole pair generation in the oxide assisted by illumination and controlled with an electrochemical set-up. Finally, a photocurrent is measured as a function of photon energy and applied potential. Wavelengths varied by 1 nm step in the range of 220–640 nm (~2–5.5 eV). Potential values were indicated with respect to the reference electrode (a mercury–mercurous sulfate electrode MSE, +0.650 V vs. standard hydrogen electrode (SHE)).

Cross section orientation maps of the oxide scales of these three experiments have been determined thanks to the precession assisted crystal orientation mapping technique, ASTAR-TEM [14], with a probe size of 1 nm and a step size of 3 nm. For that, transversal cross section thin lamellas were priority fabricated with a dual focused ion beam scanning electron microscope (FIB-SEM, Zeiss Cross Beam NVision 40). Argon or gallium ion beam polishing has also been used in order to perform cross section in the oxide scale and to be able to localize gold thanks to SEM views. ASTAR-TEM observations have been conducted on a transmission electron microscope at 200 keV (FEG-TEM, Jeol 2100F).

Table 1 AISI 441 ferritic stainless steel composition in %wt

	Fe	C	Mn	P	S	Si	Al	Ni	Cr	Cu	Mo	Sn	Nb	Ti
441	Bal	0.02	0.5	0.03	0.005	0.7	0.015	0.3	18.5	0.3	0.25	0.05	0.5	0.18

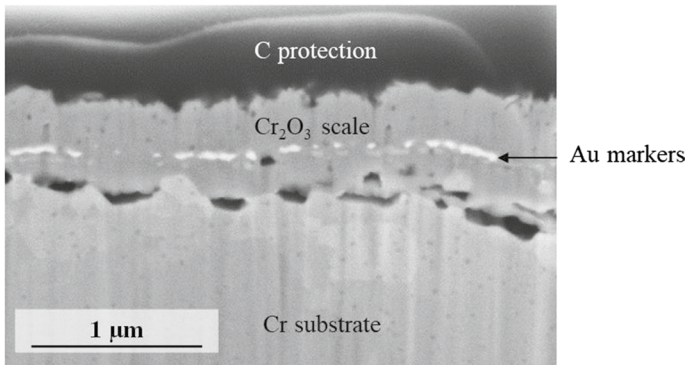


Fig. 1 Cross sectional SEM image (back-scattered electrons detector) of the Cr₂O₃ scale grown on pure golden Cr at 800 °C during 1 h at $p(\text{O}_2)$ of 10^{-14} atm

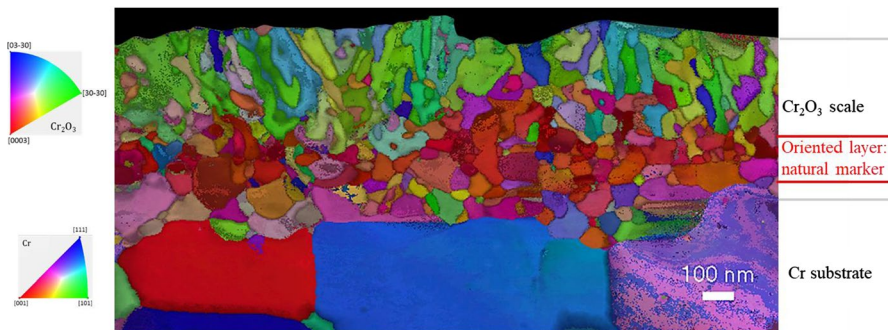


Fig. 2 TEM-ASTAR grain orientation map recorded with a probe size of 1 nm and a 3 nm step size (see color codes on the left) of Cr₂O₃ grown on pure Cr at 800 °C during 1 h at a $p(\text{O}_2)$ of 10^{-14} atm. (non-golden sample). Orientations are given along direction perpendicular to the metal/oxide interface, as in Figs. 4, 5 and 7

Results and Discussion

Pure Chromium Oxidation

FIB cross section of the oxide scale reveals that gold is found in the middle part of the oxide scale meaning that chromia is growing both inwards (anionic growth) and outwards (cationic growth) (Fig. 1). In the present case, the marker is localized in between the oxide meaning that the oxide is growing both by an anionic and a cationic way.

This result confirms what was expected [9, 15]. Indeed, ASTAR characterization had shown that the chromia morphology is duplex with an internal subscale consisted of equiaxed grains and an external subscale composed of columnar grains (Fig. 2). At the interface between the two subscales, chromia grains are oriented along the *c*-axis and appears in red on ASTAR orientation maps. This textured

chromia layer had been identified to be the first to grow (after short oxidation time and its further structural characterization [9]) and acts likely as a natural marker. From ASTAR orientation maps both inwards and outwards growth is confirmed. The growth mechanism (regarding associated PEC results) has already been proposed [9] (Fig. 3).

Photoelectrochemical experiments were performed on the samples with and without gold. Without gold, one single semiconducting contribution is revealed with n-doping (photocurrent increases with the applied potential, not shown here but previously published in [9]). The single n-chromia doping was indeed expected because of the low oxygen partial pressure equals to 10^{-14} atm. Nevertheless, when gold is priorly deposited on the Cr surface, PEC characterization reveals 2 semiconducting contributions as evidenced by the dephasing angle of 180° at 3.6 eV. For this golden oxidized Cr sample, chromia is both n-type and p-type. However, this dual semiconducting behavior is expected for oxygen partial pressure superior or equals

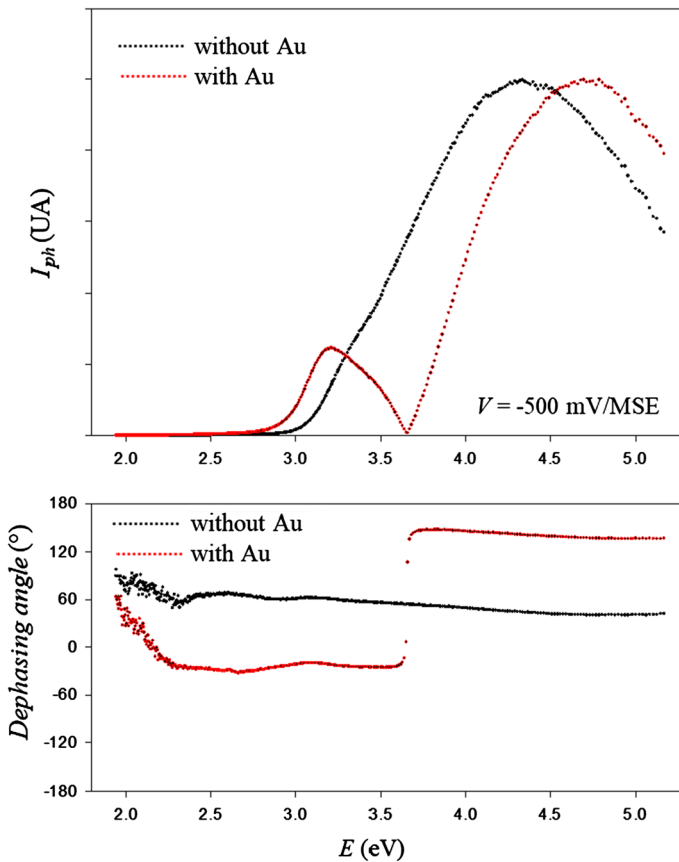


Fig. 3 Normalized photocurrent (I_{ph}) and dephasing angle versus incident light energy (E) recorded at an applied potential (V) of -500 mV/MSE from pure Cr (golden-red curves- or not -black curves-) oxidized at 800°C during 30 min at $p(\text{O}_2)$ of 5.10^{-14} , 1.10^{-13} and 5.10^{-13} atm

to 10^{-12} atm. (and for oxidation temperature between 800 and 900 °C) [10]. This experimental result clearly demonstrates that in this system gold is not inert resulting in a change of chromia conduction properties. It is rather tricky to explain the gold influence. Gold may modify the oxygen activity at the surface which could, for instance, explain the p-type semiconduction observed for chromia grown apparently at a $p(\text{O}_2)$ inferior to 10^{-12} atm. This assumption might be supported by the catalyst capability of gold nanoparticles dispersed in mesoporous Cr_2O_3 evidenced during toluene oxidation [16]. In such a case, gold may favor chromium vacancy formation at the external oxide-gas interface. In addition, it is also well known that metallic nanoparticles inside the oxide can induce plasmonic effects which modify the optical properties of the system [17–20] (i.e., the photon–matter interaction and used by glassmakers to color glasses, in particular ruby red called "purple of cassius" [21]). Therefore, if such gold nanoparticles exist within the oxide layer in the present case, it can be expected that plasmonic effects may likely alter the expected response of chromia when tested during PEC. At this step, it should be admitted that the effect of gold on the Cr/O_2 system is not well understood. Anyway, the influence of the environment on the diffusion process is known to play a key role on chromia growth mechanisms. It has been, for instance, clearly demonstrated, with a two-stage oxidation test with $^{18}\text{O}_2$ and H_2^{18}O -tracers, that chromia on NiCr model alloys grows outward in $\text{Ar}-\text{O}_2$ atmospheres at high $p(\text{O}_2)$, whereas it grows inward in $\text{Ar}-\text{H}_2-\text{H}_2\text{O}$ atmosphere, i.e., under low $p(\text{O}_2)$ and high $p(\text{H}_2\text{O})$ [22].

Even if in the present case the gold position permits to determine oxide growth direction in accordance with other experiments, gold has disturbed chromia growth by modifying the type of major point defects which diffuses (chromium vacancies and oxygen vacancies instead of chromium interstitials and oxygen vacancies at this very low oxygen activity). As a consequence, gold cannot be considered as an appropriate inert marker for oxide growth direction identification. On the contrary, the oriented chromia layer acts as a natural marker evidenced by TEM-ASTAR (Fig. 2).

NiCrMn Model Alloy Oxidation

$\text{Ni}_{74.5}\text{Cr}_{25}\text{Mn}_{0.5}$ and $\text{Ni}_{74}\text{Cr}_{25}\text{Mn}_1$ alloys oxidation leads to an oxide scale classically composed of two kinds of oxide: chromia Cr_2O_3 in the internal part and $\text{Mn}_{1+x}\text{Cr}_{2-x}\text{O}_4$ spinel in the external part ([11], Figs. 4, 5). Results concerning $\text{Ni}_{74}\text{Cr}_{25}\text{Mn}_1$ and $\text{Ni}_{74.5}\text{Cr}_{25}\text{Mn}_{0.5}$ alloys after long (100 h) and short (1 h) oxidation tests are, respectively, presented in Figs. 4, 5.

The SEM micrograph (Fig. 4a) of the priory golden sample shows that gold is found at different places inside the scale: near the internal metal/chromia interface, inside the chromia scale and at the chromia/spinel interface for the alloy oxidized during 100 h at 1050 °C and at 1 atm. With this experiment it is obviously hard to determine the possible oxide growth direction. EBSD orientation map on the non-golden sample shows that the chromia grains near the internal interface are clearly preferentially oriented along the c-axis (shown in red in Fig. 4b).

Figure 5 shows TEM-ASTAR grain orientation and phase maps of the oxide scale of $\text{Ni}_{74.5}\text{Cr}_{25}\text{Mn}_{0.5}$ oxidized under 1.97×10^{-3} atm. during 1 h. These two maps

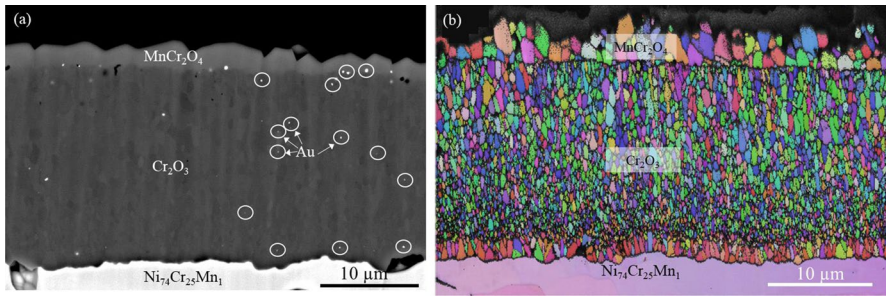


Fig. 4 **a** SEM micrographs—back-scattered electrons detector—after Ga^+ -ion milling of priory golden $\text{Ni}_{7.5}\text{Cr}_{25}\text{Mn}_1$ alloy after 100 h of oxidation at 1050 °C and at 1 atm. Some gold particles are surrounded by white circles. **b** EBSD orientation map of the corresponding non-golden sample

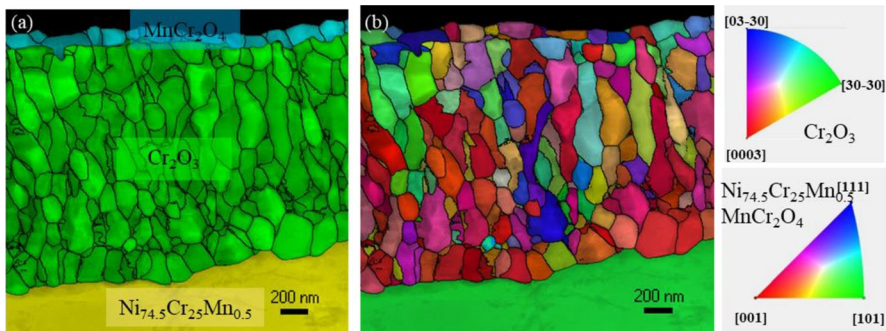


Fig. 5 TEM-ASTAR **a** phase and **b** grain orientation map (with color codes on the right) of non-golden $\text{Ni}_{7.5}\text{Cr}_{25}\text{Mn}_{0.5}$ oxidized under 1.97×10^{-3} atm. at 1050 °C during 1 h

clearly put in evidence that the external spinel is composed of only one grain in the scale thickness without preferential orientation. Chromia case is more complex to describe. Grains nearest of the metal/oxide interface are equiaxed and are preferentially oriented along the c-axis (Fig. 5b), as for $\text{Ni}_{7.4}\text{Cr}_{25}\text{Mn}_1$ oxidized a longer time. The other chromia grains do not show a preferential orientation and their morphology is slightly columnar; some of them are equiaxed.

From our knowledge on chromia morphology, it is thought that the first row of chromia grains have grown inward, whereas the other chromia rows have grown outward. The spinel growth direction is still difficult to determine with certainty, but an external growth seems the most favorable (just because a same interface for an external chromia growth and an inward spinel growth is difficult to figure out).

Ferritic Stainless Steel Oxidation

The oxide scale from 441-stainless steel oxidation is, as expected, composed once again of an internal chromia and an external $\text{Mn}_{1+x}\text{Cr}_{2-x}\text{O}_4$ spinel [23, 24] (Fig. 6a, b). A very thin and discontinuous silica layer is additionally found at the

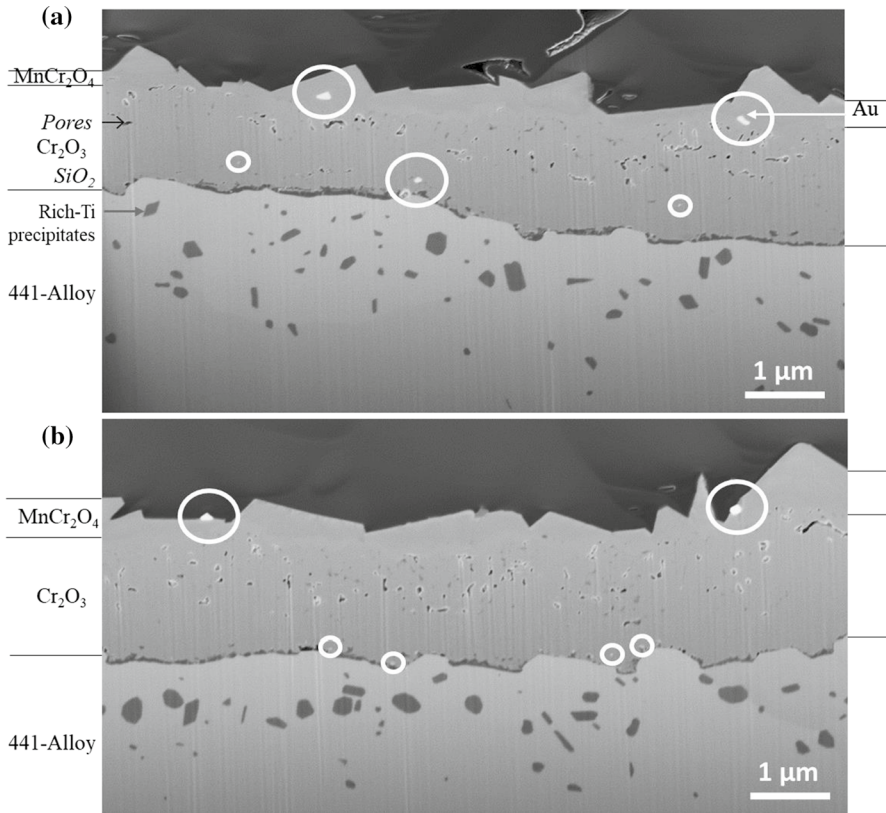


Fig. 6 a, b SEM micrographs—back-scattered electrons detector- after Ga^+ -FIB cuts of priory golden 441-stainless steel oxidized at $900\text{ }^\circ\text{C}$ during 100 h at two different places on the same sample. Gold particles are surrounded by white circles

metal/oxide interface as well as tiny pores inside chromia scale. Several FIB cuts have been achieved in order to localize gold after oxidation experiment (Fig. 6a, b). It is shown that gold can be found either at the metal/oxide interface (Fig. 6b), or inside chromia (Fig. 6a), or at the chromia/spinel interface (Fig. 6a), or at the external spinel/gas interface (Fig. 6b). Finally, gold can be found everywhere.

From TEM-ASTAR characterization of the non-golden oxidized sample during 10 h (Fig. 7), the oxide scale can be described in three main subscales:

- an internal equiaxed chromia subscale,
- an intermediate columnar chromia subscale,
- and an external spinel $\text{Mn}_{1+x}\text{Cr}_{2-x}\text{O}_4$ subscale.

In the shown example in Fig. 7, the pores (in black) separates here the equiaxed chromia subscale from the columnar one.

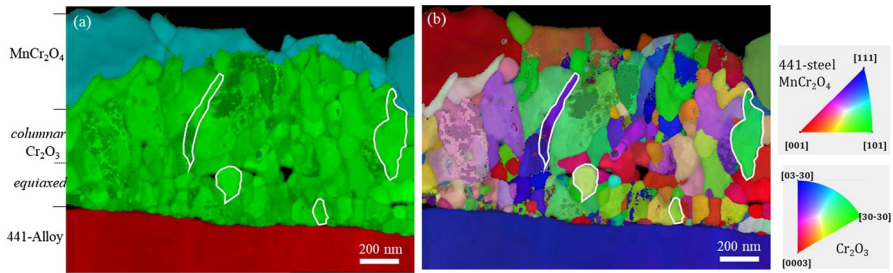


Fig. 7 TEM-ASTAR **a** phase and **b** grain orientation map (with color codes on the right) of non-golden 441 ferritic stainless steel alloy oxidized at 900 °C during 10 h (Color figure online)

In this last example, no any preferential orientation is found. However, if the chromia morphology is, as it can be believed from our previous works [9, 10, 15], linked to the oxide growth direction, it can be thought that, once again, chromia grows both inwards and outwards, whereas spinel oxide may grow outwards. Mechanisms behind will be the subject of another paper [25].

In all these examples ASTAR characterization has permitted to deduce the oxide growth direction without interfering the studied system.

Gold, a noble metal, is usually considered to be inert and is often used to sign the oxide growth direction [4, 5] but these several experiences tend to prove its non-inertia. Gold probably acts as a catalyst and modify growth mechanisms. The reliability of marker experiments for high-temperature oxidation research has been indeed several times questioned [26]. Young et al. [27] have, for instance, show that NiAl oxidizes mainly by Al outward diffusion, whereas the use of noble metal marker on NiAl prior to oxidation remains at the gas-oxide interface (and argues for an inward diffusion). Czerwinski [28] has also alerted on the gold effect with an acceleration of the oxidation rate of pure Ni. This increase is in this case explained by gold fragmentation that causes an oxide grain refinement which in turn accelerated the oxidation rate.

On NiCr(Mn) and ferritic stainless steel alloys, it has been shown that gold does not sign at all the initial metallic surface but is rather randomly distributed. A difficulty is to explain how gold particles can be found at such different places (whereas gold particles are separated by only few microns). One possibility is that gold particles are carried by the inward or the outward growing of oxide grains. Moreover, the non-simultaneous, both lateral and vertical oxide growth might explain that gold can be found nearly everywhere inside the oxide scale. This assumption is supported by an in situ characterization of chromia growth via ESEM which evidenced such gold particle displacements with oxide grain formation (Fig. 8). In this last example NiCr alloy was oxidized at 1000 °C under 1.97×10^{-3} atm. A gold particle, surrounded, by a red circle is laterally moved by chromia grains growth and begins to be recovered by chromia, whereas another gold particle surrounded by a blue circle is rapidly totally recovered by chromia. Just around gold particles remain at the top surface all along oxidation time. This is the case of the gold particle, 1 μm away, surrounded by a green circle. This *in*

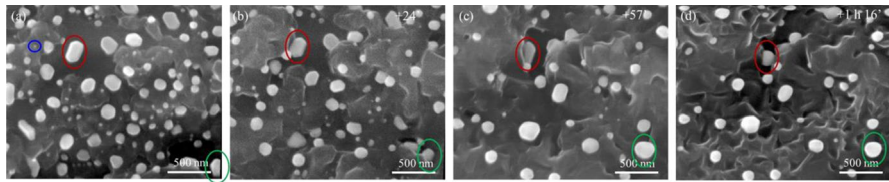


Fig. 8 ESEM oxidation (back-scattered electrons detector) of NiCr alloys under 1.97×10^{-3} atm at 1000 °C **a** beginning of the observation, **b** after 24 min, **c** after 57 min (and) after 1 h 16 min. The gold particle surrounded by a red circle is moved by the lateral chromia growth and begins to be recovered. The tiny gold particle surrounded by a blue circle is recovered by chromia growth. The gold particle, surrounded by a green circle, stays on the top of the surface, coalesces with another gold particle between **(b)** and **(c)** and finally stands on the top of the chromia external surface in **(d)**

situ characterization seems to well support our explanation about gold particles displacement during oxide growth.

Conclusion

Gold is traditionally used in the high-temperature oxidation community in order to determine oxide growth direction based on its localization in the scale. However, gold can influence chromia semiconducting properties and modifies its conduction type. Whereas non-golden pure Cr oxidized at a low oxygen partial pressure is only n-type, a golden sample becomes both n- and p-type. More importantly, gold can be found at different places after oxidation experiments on chromia-former alloys and finally does not sign the initial metallic surface. ASTAR-TEM can be an interesting alternative in order to determine oxide growth direction without perturbing the studied system. These results should alert on the non-inertia of gold markers.

Acknowledgements This work is supported by the French National Research Agency (ANR) through the PSEUDO project. The authors acknowledge the facilities, and the scientific and technical assistance of the CMTC characterization platform of Grenoble INP supported by the Centre of Excellence of Multifunctional Architected Materials "CEMAM" n°AN-10-LABX-44-01 funded by the "Investments for the Future" Program. The authors would like also to thank Florence Robaut for FIB-SEM preparation and Gilles Renou for TEM microscopy.

References

1. W. J. Quadakkers, A. Elschner, and W. Speier, H. Nickel, *Applied Surface Science* **52**, (4), 271–287 (1991).
2. S. Chevalier, G. Bonnet, G. Borchardt, J.-C. Colson, and J.-P. Larpin, *Ceramics* **61**, 177–187 (2000).
3. J. Pfeil, *J. Iron Steel Inst.* **119**, 501–547 (1929).
4. P. Sarrazin, A. Galerie, J. Fouletier, *Mechanisms of High Temperature Corrosion* (Trans Tech Publication edition, 2008).
5. D. Young, *High Temperature and Corrosion of Metals*, ed. (2008).
6. H. Sieber, D. Hesse, X. Pan, S. Senz, and J. Heydenreich, *J. Inorg. And Gal. Chem.* **622**, 1658–1666 (1996).
7. X. Ledoux, S. Mathieu, M. Vilasi, Y. Wouters, P. Del-Gallo, and M. Wagner, *Oxid. Met.* **80**, 25–35 (2013).

8. Q. Dong, G. Hultquist, G. I. Sproule, and M. J. Graham, *Corros. Sci.* **49**, 3348–3360 (2007).
9. L. Latu-Romain, Y. Parsa, S. Mathieu, M. Vilasi, A. Galerie, and Y. Wouters, *Corros. Sci.* **126**, 238–246 (2017).
10. Y. Parsa, L. Latu-Romain, Y. Wouters, S. Mathieu, T. Perez, and M. Vilasi, *Corros. Sci.* **141**, 46–52 (2018).
11. T. Perez, J. Ghanbaja, S. Mathieu, L. Latu-Romain, M. Vilasi, and Y. Wouters, *Scripta Mater.* **178**, 176–180 (2020).
12. L. Latu-Romain, Y. Parsa, S. Mathieu, M. Vilasi, and Y. Wouters, *Oxid. Met.* **90**, (3–4), 255–266 (2018).
13. L. Latu-Romain, Y. Parsa, S. Mathieu, M. Vilasi, and Y. Wouters, *Oxid. Met.* **90**, (3–4), 267–277 (2018).
14. E. Rauch and M. Véron, Automated crystal orientation and phase mapping in TEM. *Mater. Charact.* **98**, 1–9 (2014).
15. L. Latu-Romain, Y. Parsa, S. Mathieu, M. Vilasi, M. Ollivier, A. Galerie, and Y. Wouters, *Oxid. Met.* **86**, (5), 497–509 (2016).
16. Z. Wu, J. Deng, S. Xie, H. Yang, X. Zhao, K. Zhang, H. Lin, H. Dai, and G. Guo, *Microporous and Mesoporous Materials* **224**, 311–322 (2016).
17. M. Eichelbaum, K. Rademann, R. Müller, M. Radtke, H. Riesemeier, and W. Görner, *Angew. Chem. Int.* **44**, 7905–7909 (2005).
18. G. Mie, *Annalen der Physik* **25**, 377 (1908).
19. K. L. Kelly, E. Coronado, L. L. Zhao, and G. C. Schatz, *J. Phys. Chem. B* **107**, 668 (2003).
20. P. K. Jain, I. H. El-Sayed, and M. A. El-Sayed, *Nanotoday* **2**, 18 (2007).
21. W.A. Weyl, *Coloured Glasses* (The Society of Glass Technology, 1951).
22. J. Zurek, D. J. Young, E. Essuman, M. Hänsel, H. J. Penkalla, L. Niewolak, and W. J. Quadackers, *Materials Science and Engineering A* **477**, 259–270 (2008).
23. D. Nguyen, J. Zhang, and D. J. Young, *Corros. Sci.* **112**, 110–127 (2016).
24. M. R. Ardigo-Besnard, I. Popa, O. Heintz, R. Chassagnon, M. Vilasi, F. Herbst, P. Girardon, and S. Chevalier, *Applied Surface Science* **412**, 196–206 (2017).
25. T. Roy, L. Latu-Romain, I. Guillotte, B. Latouche, Y. Wouters, *Oxid. Met.*, to be published.
26. R. Prescott and M. J. Graham, *Oxid. Met.* **38**, (3/4), 1992 (233–254).
27. E. W. A. Young, H. E. Bishop, and J. H. W. De Wit, *Surf. Interface Anal.* **9**, 163–168 (1986).
28. F. Czerwinski, *Acta Materialia* **48**, (3), 721–733 (2000).

Publisher's Note Springer Nature remains neutral with regard to jurisdictional claims in published maps and institutional affiliations.